

A Diffusion-based 3D FEM Analysis for Assessment of Reactivity Change due to Core Deformation in an SFR

Woong Heo and Yonghee Kim*

Korea Advanced Institute of Science and Technology (KAIST), 291 Daehak-ro, Yuseong-gu, Daejeon, Korea, 34141

*Corresponding author: yongheekim@kaist.ac.kr

1. Introduction

In previous work [1], the Galerkin finite element method (GFEM) based on 2D diffusion analysis has been applied to estimate the reactivity changes due to assembly deformation. The feasibility of utilizing low-order approximation in meshing and shape function has been evaluated, and it has been shown that the GFEM-based diffusion analysis with low-order approximation can well predict the reactivity changes due to the geometric perturbation in an SFR. However, a 2D deformation in the assembly is limited to a moving hexagonal shape. Furthermore, it cannot consider deformations like irregular axial expansion and flowering. Therefore, an extension from 2D to 3D is necessary.

The main purpose of this study is to evaluate the deformation-related reactivity changes by directly modeling 3D local deformations of assemblies in an SFR after extending the 2D GFEM-based diffusion code into the 3D code. Similar to the previous 2D study, multi-group diffusion equation based on GFEM with low-order approximations (linear shape function and 4-node tetrahedral element) has been used for estimating reactivity changes due to core deformation in an SFR.

2. Finite element method for multi-group diffusion equation with unstructured tetrahedral element

The multi-group diffusion equation without external neutron source is given in Eq. (1). In Eq. (2), neutron flux is expressed by the combination of linear shape functions in each tetrahedral element (Fig. 1).

$$-D_g \nabla^2 \phi_g + \Sigma_{rg} \phi_g = \left[\begin{array}{c} \sum_{g'=1}^{G, g' \neq g} (\Sigma_{sg' \rightarrow g} \phi_{g'}) \\ + \frac{1}{k_{eff}} \chi_g \sum_{g'=1}^G (v_{g'} \Sigma_{fg'} \phi_{g'}) \end{array} \right], \quad (1)$$

$g = 1, 2, \dots, G$

$$\phi_g(x, y, z) = \sum_{e=1}^E \left[\begin{array}{c} \phi_{g,1} L_1(x, y, z) + \phi_{g,2} L_2(x, y, z) \\ + \phi_{g,3} L_3(x, y, z) + \phi_{g,4} L_4(x, y, z) \end{array} \right] \quad (2)$$

$E =$ total # of Element

By using the Galerkin approximation and weak form formulation, the multi-group diffusion equation can be

expressed by the terms of shape functions as shown in Eq. (3).

$$\left(\begin{array}{c} \sum_{e=1}^E \left[D_{g,e} \int_{V_e} \nabla L_j \cdot \nabla L_i dV \right] + \sum_{e=1}^E \left[\Sigma_{rg,e} \int_{V_e} L_j L_i dV \right] \\ - \sum_{e=1}^E \sum_{u=1}^U \left[\int_{A_e^u} \gamma_u L_j L_i dA \right] \end{array} \right) \phi_{g,i}$$

$$= \left(\begin{array}{c} \sum_{g'=1}^{G, g' \neq g} \left(\Sigma_{sg' \rightarrow g} \int_{V_e} L_j L_i dV \right) \phi_{g',i} \\ + \frac{1}{k} \sum_{g'=1}^G \left(\chi_{g,e} (v_{g'} \Sigma_{fg'}) \int_{V_e} L_j L_i dV \right) \phi_{g',i} \end{array} \right) \quad (3)$$

where $j, i = 1, 2, \dots, J$

$J =$ total # of Nodes (Global node index)

$U =$ # of Boundary surfaces of D_e ,

$$\gamma_u = \left\{ \begin{array}{l} \frac{1}{2} (\alpha_{g,u} - 1), \text{ BC at surface } 'u': A_e^u \\ 0, \text{ otherwise} \end{array} \right\}$$

$$\alpha_{g,u} = \frac{J_g^-(in)}{J_g^+(out)} \text{ at surface } 'u': A_e^u,$$

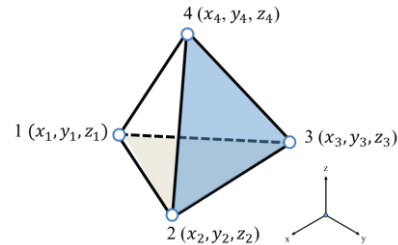


Fig. 1. Tetrahedral Element

Group-wise neutron loss and production matrices (LHS and RHS, respectively) can be generated from Eq. (3) by the combination of node indices in each element. In this study, a 3D GFEM solver has been implemented by using the conjugate gradient (CG) method as an iterative solver. Effective multiplication factors in steady state (before and after geometric perturbation) have been obtained by the implemented code and reactivity changes due to core deformation have been calculated.

3. Mesh control for assembly deformation

In this study, the open source program GMSH [2] has been utilized for the whole core modeling including assembly deformation. The geometry of any assembly

consists of unit hexagonal cell. Two types of hexagonal cell have been chosen for this study and they are shown in Fig. 2. One (1-layer modeling) is composed of six triangular prisms and each prism can have an independent material. The other (2-layer modeling) has six triangular prisms and six trapezoidal prisms and an independent material can be assigned for each prism. In this study, a homogeneous mixture of duct and sodium gap is used for a material in the trapezoidal prism.

It is possible to move intersecting points between prisms in a hexagonal cell for reflecting geometrical perturbations. For a hexagonal cell displacement, the 1-layer modeling has a total of 14 nodal points (top: 7, bottom: 7) and 2-layer modeling has a total of 26 nodal points (top: 13, bottom: 13).

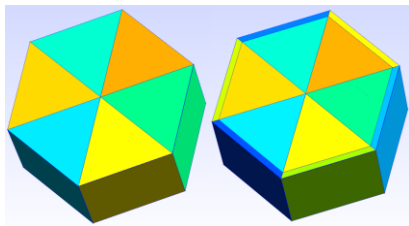


Fig. 2. Unit hexagonal cell of 1-layer modeling (left) and 2-layer modeling (right).

The same geometries in GMSH before and after perturbations have been used for reference Serpent2 [3] calculations (Monte Carlo simulation code). The output format (.msh) from GMSH has been converted into the OpenFOAM format which are available in Serpent2 for the reference core modeling.

4. Reference core model description and multi-group cross section generation

A 3D prototype Gen IV sodium-cooled fast reactor (PGSFR), shown in Fig.3, has been chosen as the reference core model [4]. Fig. 4 shows axial configuration of fuel assembly and control assembly.

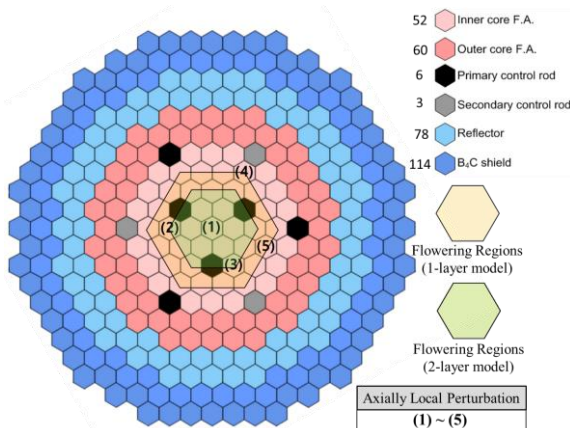


Fig. 3. Radial core configuration of PGSFR and selected regions (or assemblies) for core perturbations.

In this study, 9-group cross sections have been generated from TRANSX/TWODANT code in the conventional way (RZ-flux weighting) and the generated group constants were used for 3D GFEM analysis. A generated 150-group library (MATXS format) from ENDF/B-VII.0 was used to condense fine-group cross sections into 9-group constants. Reference calculations have been conducted using Serpent2.1.29 with ENDF/B-VII.0 library.

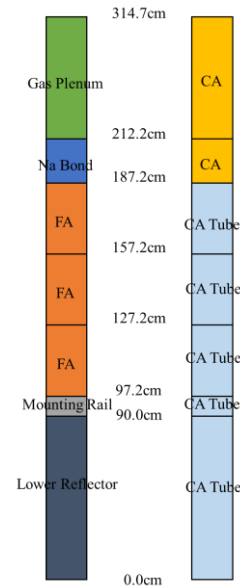


Fig. 4. Axial assembly configuration of PGSFR (left: fuel assembly, right: control assembly).

In this study, only the atomic number densities of the deformed prisms in a hexagonal cell have been modified to compensate for the change of macroscopic cross sections. In other words, it is assumed that microscopic cross sections and fission spectrum are not changed after assembly deformations because they are not strongly affected by small perturbations in a fast reactor, except in extreme deformation scenarios. The atom number densities are simply weighted by a volume ratio as shown in Eqs. (4) and (5).

$$\frac{V_{original}}{V_{perturbed}} = w_{ND}, \quad V = \text{Volume of prism} \quad (4)$$

$$N_{perturbed} = w_{ND} \times N_{original}, \quad N = \text{Atom number density} \quad (5)$$

5. Deformation scenarios

The core deformation types in this study consist of 1) irregular axial expansion and 2) local flowering depending on the modeling of a unit hexagonal cell. A total of four scenarios are summarized in Table I.

Five positions (1) ~ (5) in the inner core region have been selected for irregular axial expansions (scenario 1 and 3) as shown in Fig 3. It is assumed that total height

of assembly does not change after axial expansion. It should be mentioned that the top surfaces of axially expanded assemblies (2) ~ (5) are slanted. Fig. 5 shows detailed information about axial displacement at each nodal point. Only the axial displacements at nodes 8~13 are applied to 1-layer modeling.

Table I. Core deformation scenarios

Scenarios	Deformation type	Modeling
1	Irregular Axial Expansion	1-layer
2	Local Flowering	1-layer
3	Irregular Axial Expansion	2-layer
4	Local Flowering	2-layer

The local flowering occurs from hexagonal ring 1 to ring 3, and radial movements of top surfaces start from a height of 187.2 cm to a height of 314.7 cm as shown in Fig. 6. In other words, actual volume changes after a flowering occur from 157.2 cm to 314.7 cm in height. The flowering is controlled by the maximum displacement of the surface at a height of 314.7 cm. The degree of displacement of the other surfaces (187.2 cm and 212.2 cm in height) is defined as the product of the maximum displacement at the top surface and a height ratio between the top surface and the target surface.

The modeling of flowering using the 1-layer hexagonal cell is rather restricted than that of using the 2-layer cell because any radial expansion (contraction) or displacement of assembly involves another contraction (expansion) of neighboring assemblies. For this reason, in the case of 1-layer modeling, additional contractions at hexagonal ring 4 have been applied because of expansions at hexagonal ring 3. In the case of 2-layer modeling, only inner hexagon surfaces in ring 1~3 have been shifted outward for flowering. There is no change of axial height for both 1-layer and 2-layer flowering.

For the 1-layer modeling, the top surface of ring 1 radially expands by 0.45 cm (i.e. 0.90 cm in pitch size), and the top surfaces of ring 2 and 3 radially expand by 0.30 cm and 0.15cm respectively. The radial expansions start from ring 1 to ring 3 in order. As already mentioned, the contraction caused by the expansion of ring 3 is applied to ring 4.

It is possible to set a deformation model so that the influence of the assembly deformation does not force the adjacent assemblies to expand or contract in 2-layer modeling. For local flowering, there is no deformation or expansion in ring 1 and the hexagon surfaces at top level (314.7 cm) have been shifted by 0.3 cm for ring 2 and 0.4 cm for ring 3. There is no deformation of inner hexagon shape for local flowering in the case of 2-layer modeling.

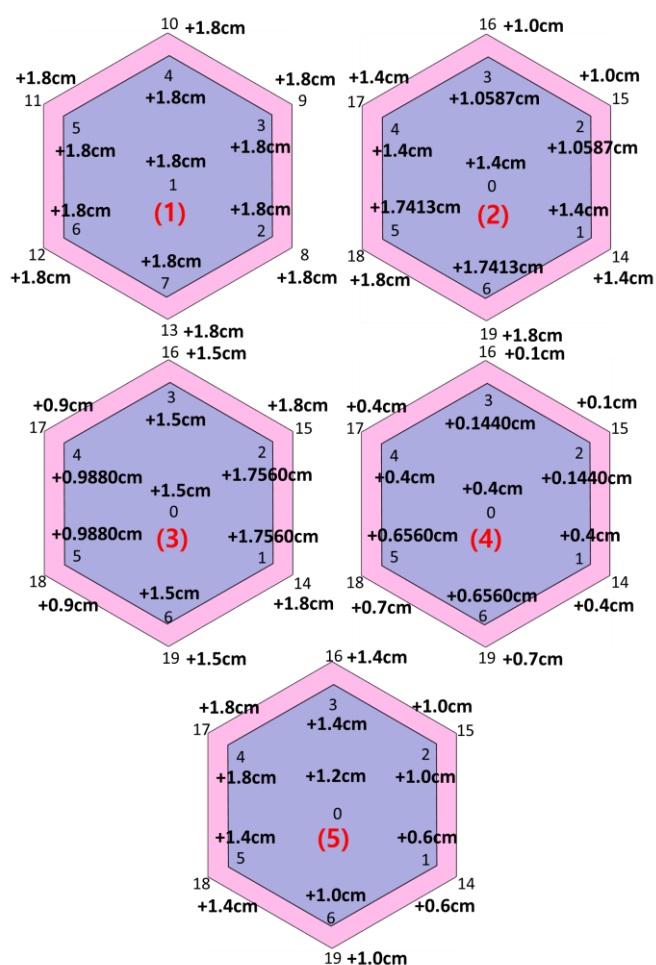


Fig. 5. Axial displacement of nodal points on top surface of unit hexagonal cell (fuel assemblies)

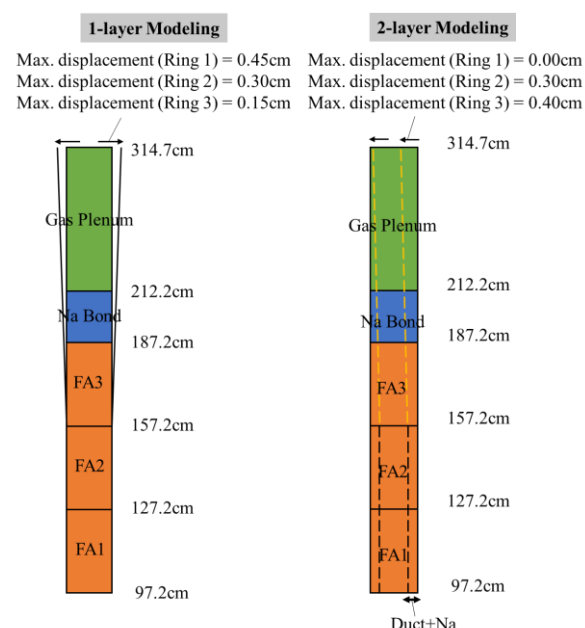


Fig. 6. Local flowering for 1-layer and 2-layer modeling

6. Numerical results

The Serpent2 and GFEM results of 3D PGSFR for each deformation scenario are shown in Table II and III respectively. All reference calculations have 0.56 pcm as standard deviations using 4,000,000 histories per cycle with total 5,000 cycles (1,000 inactive). A total of 84 and 40 cores were used for Serpent2 calculation (hybrid MPI) and GFEM (OpenMP) calculations respectively.

Table II. Reference results of 3D PGSFR

Reference (Serpent2.1.29) using ENDF/B-VII.0				
Deformation scenario	Time (day)	k-eff	$\Delta\rho$ (pcm)	1σ of $\Delta\rho$ (pcm) (% of $1\sigma/\Delta\rho$)
Reference State of 1,2	2.07	1.085030	-	-
1	2.08	1.084834	-16.68	0.67 (4.02)
2	3.21	1.085012	-1.52	0.67 (44.08)
Reference State of 3,4	2.86	1.086267	-	-
3	2.86	1.086042	-19.13	0.67 (3.50)
4	3.14	1.086260	-0.63	0.67 (106.35)

Table III. GFEM results of 3D PGSFR

3-D GFEM, 9-group constants			
Deformation scenario	Avg. # of elements ^(a)	$\Delta\rho$ (pcm)	Avg. Time (sec) ^(b)
1	1073331	-16.88	998
	1384476	-16.81	1239
	1466678	-16.99	1471
	2943771	-16.81	2952
	3649389	-16.72	3603
	6213725	-16.66	6537
2	9652291	-16.67	10283
2	4273473	-0.92	4583
3	4925330	-16.99	16662
	8972265	-17.05	21286
4	4378724	-1.93	8493

(a): average number of elements before and after perturbation

(b): average calculation time before and after perturbation.

In the case of scenario 1, it is shown that the reactivity changes due to core deformation are not significantly dependent on mesh refinement (according to the number of tetrahedral elements) by virtue of error cancellation in the calculation of reactivity change. The impact of error cancellation is also observed in the scenario 3, where the difference in reactivity change is only 0.6 pcm even though the number of elements is nearly doubled.

As shown in Table II, since the standard deviations of reactivity changes in scenario 2 and 4 are about 44% and 106% respectively, it is difficult to say that the small reactivity changes are in reliable ranges as reference values. Despite the large uncertainty of reference values in the two cases, the errors of reactivity changes calculated by 3D GFEM are less than 2.2 pcm for all cases. This indicates that the GFEM-based

diffusion analysis using low-order approximations can be utilized to evaluate the reactivity changes in acceptable precision even for a small geometric perturbation. In addition, the computing time of GFEM is much shorter than that of Monte Carlo simulations, even though the optimization of 3D GFEM code for computational performance is not conducted.

7. Conclusions

In this study, the estimation of reactivity changes due to core deformation has been conducted with GFEM-based diffusion analysis for the 3D PGSFR. The reactivity changes were evaluated using the multi-group GFEM-based diffusion equation (9-group constants in this study), and the results from 3D GFEM were compared with Monte Carlo results (Serpent2.1.29) which used continuous energy cross sections.

Two types of unit hexagonal cells, capable of considering assembly deformation, have been suggested for the whole core modeling. Using these two types of modeling, the estimation of reactivity changes has been performed for four scenarios of core deformation. The differences of evaluated reactivity changes between 3D GFEM and reference were less than 2.2 pcm for all scenarios.

In conclusion, due to the effect of error cancellation, we found that the GFEM-based diffusion analysis in an SFR with low-order approximation has good feasibility to efficiently estimate reactivity changes caused by geometric deformation.

8. Acknowledgements

This work was supported by the National Research Foundation of Korea (NRF) Grant funded by the Korean Government (MSIP) (NRF-2016R1A5A1013919).

REFERENCES

- [1] Woong Heo and Yonghee Kim, Diffusion-based Finite Element Method to Estimate the Reactivity Changes due to Core Deformation in an SFR, *Nuclear Science and Engineering* 189(1), 41-55, 2017.
- [2] C. Geuzaine and J.-F. Remacle, Gmsh: a three-dimensional finite element mesh generator with built-in pre- and post-processing facilities, *International Journal for Numerical Methods in Engineering* 79(11), pp. 1309-1331, 2009.
- [3] J. Leppänen, Serpent – a Continuous-energy Monte Carlo Reactor Physics Burnup Calculation Code, *VTT Technical Research Centre of Finland*, Mar. 6, 2013
- [4] KOREA ATOMIC ENERGY RESEARCH INSTITUTE and SODIUM-COOLED FAST REACTOR DEVELOPMENT AGENCY, *The 3rd International Technical Review Meeting for Prototype Gen IV SFR (PGSFR) Development in Korea*, compiled files, 2014